Geophysical Research Letters

RESEARCH LETTER
10.1029/2019GL082414

Extreme Convective Storms Over High-Latitude Continental Areas Where Maximum Warming Is Occurring

Robert A. Houze Jr[1,2], Jingyu Wang[2], Jiwen Fan[2], Stacy Brodzik[1], and Zhe Feng[2]

[1]Department of Atmospheric Science, University of Washington, Seattle, WA, USA, [2]Atmospheric Sciences and Global Change Division, Pacific Northwest National Laboratory, Richland, WA, USA

Key Points:
- The GPM satellite observes a common occurrence of extremely intense convective systems at high latitudes, where the maximum surface warming has been occurring
- The three-dimensional radar reflectivity structure and environmental variables of the high-latitude extreme convective systems are revealed
- The occurrence frequency and intensity of high-latitude extreme convective storms could increase in the future warming climate

Correspondence to:
R. A. Houze Jr and J. Fan,
houze@uw.edu;
jiwen.fan@pnnl.gov

Citation:
Houze, R. A., Jr, Wang, J., Fan, J., Brodzik, S., & Feng, Z. (2019). Extreme convective storms over high-latitude continental areas where maximum warming is occurring. *Geophysical Research Letters*, *46*, 4059–4065. https://doi.org/10.1029/2019GL082414

Received 9 FEB 2019
Accepted 29 MAR 2019
Accepted article online 3 APR 2019
Published online 15 APR 2019

Abstract Deep convective storms play a key role in severe weather, the hydrological cycle, and the global atmospheric circulation. Historically, little attention has been paid to the intense convective storms in the high latitudes. These regions have been experiencing the largest increases of mean surface temperature over the last century. The Global Precipitation Measurement core satellite, which features a space-borne Dual-frequency Precipitation Radar providing near-global coverage (65°S to 65°N), has made it possible to establish the occurrence of convective storms at high latitudes. Analysis of the three-dimensional radar echoes seen by Global Precipitation Measurement over a 5-year period (2014–2018) shows that extremely intense deep convective storms do occur often during the warm season (April–September) in the high-latitude continents where the increase of surface temperature has been greatest. The associated thermodynamical environments suggest that high-latitude extreme convection could be more common in a continually warming world.

Plain Language Summary Over the last century, the North Hemisphere high-latitude continental regions (Siberia, northern Europe, and northern Canada) have experienced the greatest surface temperature increase on Earth. Launched in 2014, the Global Precipitation Measurement core observatory satellite with Dual-frequency Precipitation Radar has been providing observations at these high latitudes. These observations show that extreme convective storms are occurring in these high-latitude continental regions. Five years of these satellite radar data show statistics of these convective systems based on their three-dimensional radar reflectivity structures. The patterns of occurrence are consistent with the statistics of reanalysis data on the surface wind, temperature, and humidity as well as thermodynamic profiles during the times of satellite-observed storms.

1. Introduction

Deep convective storms—cumulonimbus clouds reaching to great altitudes and producing heavy rain, hail, and wind—are well known at lower and middle latitudes. Groenemeijer et al. (2017) have documented occasional ground observations of such severe weather in Europe and have shown that environmental conditions supportive of severe convective weather occur from time to time in these high latitudes. Recent work has also shown that surface warming is greatest at high latitudes (e.g., Wuebbles et al., 2017) and that convective available potential energy (CAPE) should increase under warming conditions (Sobel & Camargo, 2011). The questions arise: (1) What is the global picture of the extreme convective storms over all high-latitude regions? And (2) is there a correspondence between high-latitude convective storms and increased mean surface temperature?

To answer these questions, a global climatological documentation of extreme convective storms at high latitudes using satellite observations of such storms is needed. Radar aboard a satellite provides three-dimensional observations of storm structure that can both indicate the occurrence of intense convection and be mapped climatologically over the globe. By using 16-year data set collected by the Tropical Rainfall Measuring Mission satellite, Houze et al. (2015) presented the global distribution of the probability of various convective systems at low latitudes (35°S–35°N). Since 2014, the Global Precipitation Measurement (GPM) core observatory satellite, which orbits between 65°N and 65°S, has Dual-frequency Precipitation Radar (DPR) on board and provides radar data similar to that supplied by the now defunct Tropical Rainfall Measuring Mission satellite, but extending into the high-latitude region where surface

warming of Earth has been greatest. The GPM data allow for an objective global census of deep convection at high latitudes in the period since 2014. Such an investigation is highly important for understanding weather and climate change in a warming world. In this article, we (1) examine the occurrence of the extreme convective storms at high latitudes seen by GPM since 2014 and show the correspondence between the occurrence of those strong storms and the greatest surface warming and (2) determine statistics of the environmental variables associated with the extreme convective storms seen at high latitudes by GPM.

2. Data and Methods

The GPM DPR data provided by the National Aeronautics and Space Administration (Iguchi et al., 2017) are divided into convective, stratiform, and other echoes according to the method of Awaka et al. (1997). To analyze the occurrence of intense convective storms at high latitudes, we examine the convective radar echoes with the methodology of Houze et al. (2007, 2015), who take advantage of the three-dimensional radar structure seen by satellite-borne radar to define three categories of extreme convective radar echo. A convective cloud system can be extreme in either vertical or horizontal scale. According to this methodology, a deep convective core (DCC) is a three-dimensional echo object consisting entirely of echo ≥40 dBZ extending to ≥10 km in maximum height, a wide convective core (WCC) is a three-dimensional echo object consisting entirely of echo ≥40 dBZ and covering ≥1,000 km^2 in horizontal dimension, and a deep and wide convective core (DWC) satisfies both criteria. To obtain the occurrence and location of the extreme convective storm metrics DCC, WCC, and DWC, the native GPM radar reflectivity data are interpolated to Cartesian coordinates, and an algorithm is applied on the interpolated data to locate the echo objects satisfying the above criteria. The locations of the DCCs, WCCs, and DWCs are then plotted geographically. The interpolated GPM reflectivity data and the results of applying the algorithms are available online (http://gpm.atmos.washington.edu/).

Ideally, we would like to identify the occurrence of mesoscale convective systems (MCSs; Houze, 2004, 2018), which are the most extreme form taken by deep convection in the atmosphere. MCSs are not only manifestations of convection of great vertical dimension but they also are entities of extensive horizontal dimension—that is, they are deep convection that has grown upscale. However, MCSs have lifetimes of many hours, and to identify them requires tracking convection in time (e.g., Feng et al., 2016), which cannot be done with the snapshots of data provided by GPM. Work in progress by some of the authors of this paper is aimed at correlating trackable geosynchronous satellite and ground-based radar with GPM radar data metrics that may provide a way to identify MCSs from GPM data. However, in lieu of such a methodology, we interpret the WCCs and DWCs as belonging to storms that are likely at least similar to MCSs in that they not only contain intense convective cores but those cores have grown upscale to mesoscale proportions.

In order to relate the occurrence of extreme convective storms seen by GPM to the global warming pattern revealed by Wuebbles et al. (2017), we have analyzed the data from the Merged Land-Ocean Surface Temperature Analysis data from the National Oceanic and Atmospheric Administration National Climatic Data Center data archive online (https://www.ncdc.noaa.gov/dataaccess/marineocean-data/noaa-global-surface-temperature-noaaglobaltemp; Vose et al., 2012).

In addition to determining the locations of radar echoes containing DCCs, WCCs, and DWCs, we obtain a statistical view of the characteristics of the large-scale environments in which these storms are located. To characterize these environments, we analyze 6-hourly ERA-Interim reanalysis data (Dee et al., 2011). These data have a grid spacing of 0.75°. We used the data nearest in time prior to events detected by the GPM and location to the centers of the events. In addition, we excluded soundings that appeared to be in cloud (temperature equal to dew point) and thus not likely to be representative of the large-scale environment.

3. Occurrence of Extreme Convective Storms at High Latitudes and Their Collocation With Largest Surface Warming

Figure 1 contains examples of three GPM DPR radar echoes observed north of 60° latitude. The first column of images in the figure illustrates a storm containing an echo core classified as a DCC, the second column show a storm containing a DWC, and the third column is for a storm containing a WCC. The top row shows the GPM DPR echo pattern in plan view with the identified echo cores DCC, DWC, and WCC shaded red.

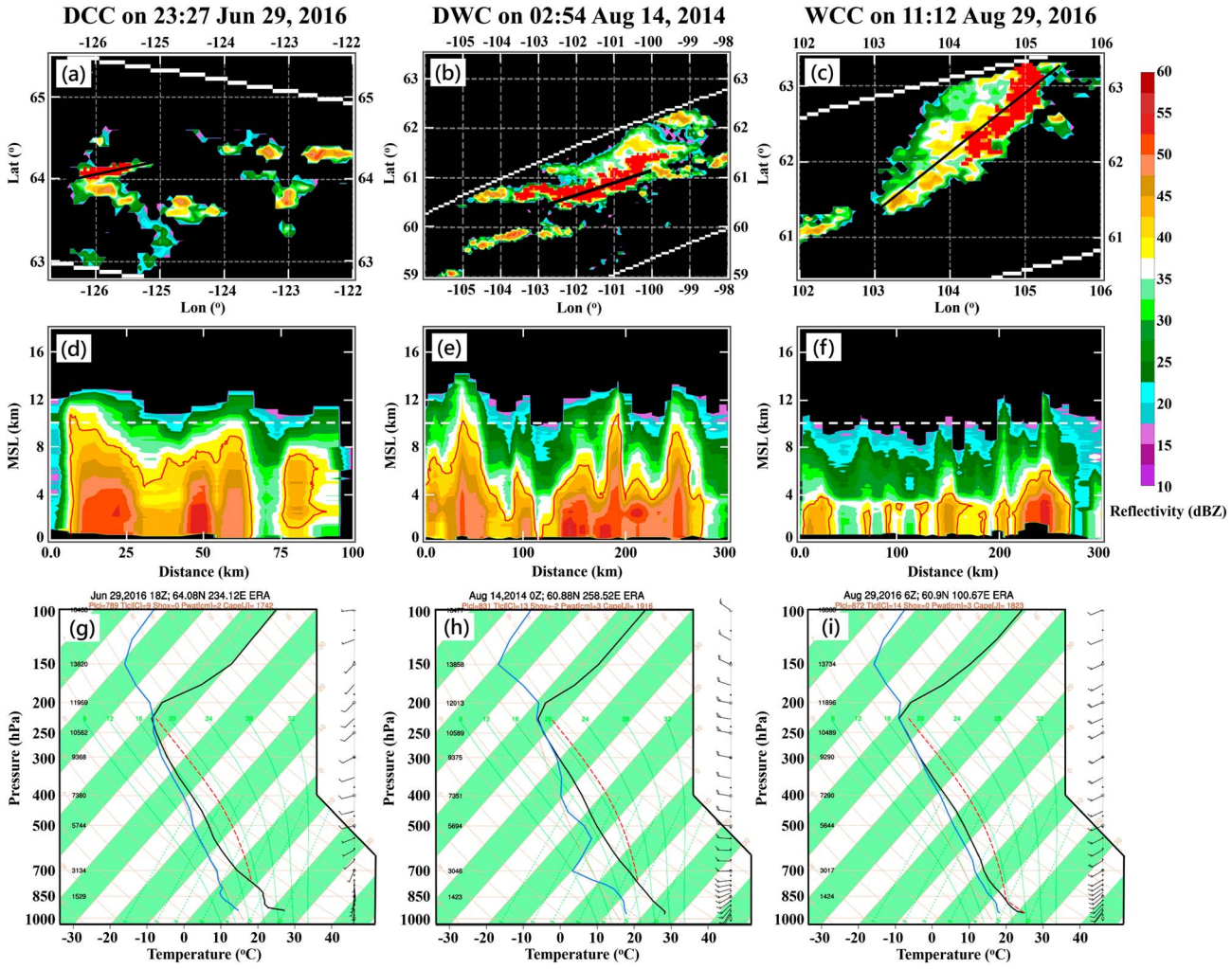

Figure 1. Examples of each of the types of extreme convective storms identified at high latitudes in this study. The top row shows the plan view of Global Precipitation Measurement Dual-frequency Precipitation Radar reflectivity (a–c); the middle row contains vertical cross sections along the black lines shown in plan view (d–f); and the bottom row shows soundings derived from ERA Interim reanalysis data in the vicinity of the storms (g–i). The left column illustrates a storm containing a deep convective core (DCC), the middle column a storm containing a convective core that is both deep and wide (DWC), and the right column a storm containing a wide convective core (WCC). In the plan view sections, echo cores designated by the Global Precipitation Measurement archive as convective are shaded in red. In the vertical cross sections (d–f), the 40-dBZ reflectivity contour is highlighted in red.

The corresponding environmental conditions are derived from reanalysis data and shown in the bottom row of the figure, which will be discussed further in section 4. The vertical cross sections show that in both the DCC and DWC, the 40-dBZ echo reaches an altitude of 10 km, but the weaker echo and cloud containing the echo core extend much higher, at least to 12–13 km (Figures 1d and 1e). The WCC illustrated in Figure 1f shows 40-dBZ echo up to only about 6 km, but 30-dBZ echoes can reach higher than 10 km altitude. As noted by Liu and Liu (2016), these can extend to great heights and likely affect the stratosphere at these high latitudes where the tropopause is at about 12 km, as can be seen in the bottom row of panels.

Application of the convection classification algorithms identifying DCCs, WCCs, and DWCs to the GPM data obtained in the 60–65°N latitude belt for the months April–September 2014–2018 showed 29 DCC, 21 DWC, and 174 WCC objects, and all of them occurred over Canada and Asia, not over the Atlantic and Pacific Oceans (Figure 2b). The WCC is the most common type, but the number of DCCs and DWC elements is significant, suggesting that convection over such high latitudes can be very intense, with strong cells sometimes penetrating the tropopause and impacting stratosphere composition. As a sensitivity test, we reran the echo-object algorithm for the 60–65°N latitude belt using 8 km rather than 10 km to determine if a three-

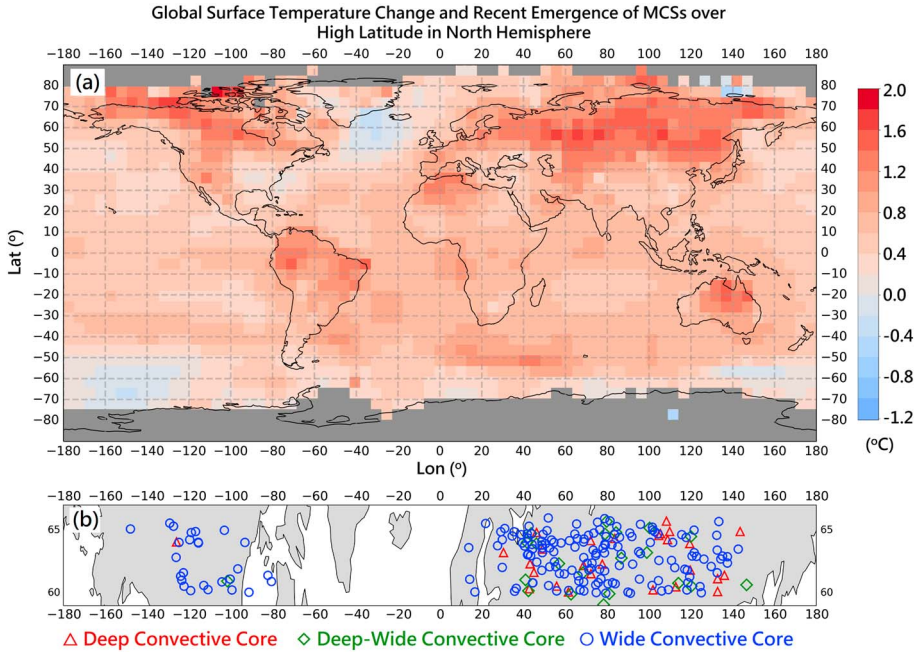

Figure 2. (a) Global surface temperature change (°C) for the period 1986–2017 relative to 1901–1960 using the data from National Oceanic and Atmospheric Administration Merged Land-Ocean Surface Temperature Analysis and (b) distribution of different types of convective systems at high latitudes determined from data of the Global Precipitation Measurement Dual-frequency Precipitation Radar during the period of 2014–2018 warm seasons (April–September). MCS = mesoscale convective systems.

dimensional echo ≥40 dBZ qualified as DCC or DWC. With this lower height requirement, the number of DCC and DWC events jumped to 931 and 86, respectively, all over land. This change in criterion did not modify the basic pattern of extreme convective occurrence shown in Figure 2b, but it indicated many more DCCs and DWCs if the top of the three-dimensional 40+ dBZ echo objects are required only to get to 8 km rather than 10 km altitude. In other words, a lot of convective storms of great vertical and horizontal extent are now occurring over land in the 60–65°N latitude belt. Even with this lower height threshold, a 40-dBZ echo core of these dimension is a very intense convective entity.

Most importantly, the extreme convective storms identified by the GPM DPR are collocated with the maximum surface warming (compare Figures 2a with 2b). Figure 2a shows the observed global surface temperature anomaly for the period 1986–2017 relative to 1901–1960. The global mean surface temperature increased by 0.7 °C; however, the mean temperature rise in the 60–65°N latitude band was 0.9 °C, and over the high-latitude landmasses of the Northern Hemisphere, the surface temperature has risen in some locations as much as 1.9 °C. Meanwhile, no such sharp increases have been occurring over high-latitude oceans in either the Northern or Southern Hemisphere.

Not only do the extreme convective storms occur where warming has been greatest but they also occur at the warmest time of year. Within the April–September window, only one of the 224 extreme convective storms we identified occurred in April, three in May, and one in September. All the rest occurred in the months of June and July. Almost all of the deepest convective storms (47 out of 50 of the DCCs and DWCs) occurred in June and July, the time of year when high-latitude solar heating is maximum. Extreme convection of large horizontal dimension (though not quite as deep) continued occurring for an additional month; 69 WCCs occurred in June, 59 in July, and 42 in August. As solar heating wanes in September, the intense storm occurrence dropped off sharply, to nearly zero.

4. Environmental Variables Corresponding to High-Latitude Convective Storms

To obtain a statistical view of the characteristics of the environments of high-latitude extreme convection, we used the ERA-Interim reanalysis data nearest in time prior to the events and location to the centers of

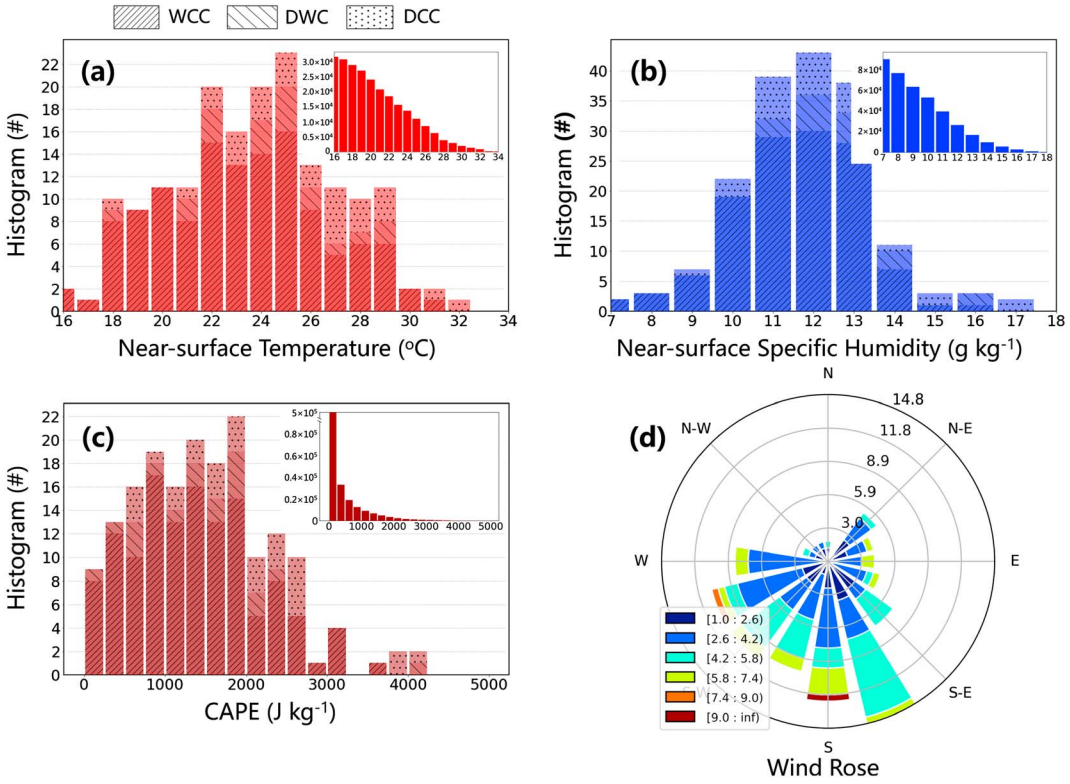

Figure 3. Histograms of (a) surface temperature, (b) surface specific humidity, (c) CAPE, and (d) surface wind direction and speed (in unit of m/s) for the intense convective events identified by the Global Precipitation Measurement Dual-frequency Precipitation Radar during the period of 2014–2018 warm seasons (April–September). The histograms from WCC, DWC, and DCC in (a)–(c) are stacked. In the upper right of (a), (b), and (c), the histograms of all the data during the analysis period in the analysis region are shown in the inset. DCC = deep convective core; WCC = wide convective core; DWC = deep and wide convective core; CAPE = convective available potential energy.

the events for all 224 GPM-observed high-latitude convective storms, excluding soundings that appeared to be in cloud (temperature equal to dew point) and thus not representative of the large-scale environment. The histograms in Figures 3a–3c show that surface temperatures in the vicinity of extreme convective events at high latitudes tend to be in the twenties in degrees Celsius; the mean value is 23.1 °C with a standard deviation of 3.4 °C. The specific humidity at the surface is mostly over 10 g/kg. These warm and humid surface conditions are associated with relatively high maximum CAPE (Moncrieff & Miller, 1976) values with a mean of 1,480 J/kg and standard deviation of 843 J/kg. The distribution of the environmental variables among WCC, DWC, and DCC is rather similar, although DCCs tend to occur in a slightly warmer, moister environment with higher CAPE than WCC. The near surface temperature, humidity, and CAPE associated with these extreme storm events are distinctly larger than the mean conditions averaged over all data (see insets of Figures 3a–3c). The upper-level temperature distribution seen in the ERA Interim reanalysis fields (not shown) is found to have high temperature anomalies associated with these extreme convective storms, indicating that the extreme convective storms at high latitudes are not associated with intrusions of cold air aloft. A detailed examination of the synoptic situations associated with extreme convective storms at high altitudes would be a valuable follow-on to this study.

The radar echo objects were detected at various times of day, and GPM provides only snapshots, so the diurnal variability cannot be readily analyzed. However, 60% of the events occurred between 1300 and 2100 local time, which would be the warmest time of day. In the most extreme case, a CAPE value of 4,000 J/kg was observed, a value rarely reached even over the Great Plains of the United States (Gartzke et al., 2017; Xie et al., 2014). The wind rose in Figure 3d shows that the surface flow into the convective regions almost always has a southerly component to advect the warm moisture-laden air into the region where storms are occurring.

5. Conclusions and Discussion

In this study, we have used the GPM DPR data to show that deep and intense convection has indeed been occurring over high-latitude continental regions where surface temperatures have been steadily increasing during the last few decades. In addition, we have used global reanalysis data to gain understanding of the conditional instability, and surface wind and temperature, corresponding to occurrences of these intense deep convective clouds at high latitudes.

More specifically, the DCC, WCC, and DWC echo objects derived from GPM DPR measurements show that extreme forms of cumulonimbus convection occur over high-latitude continental regions in the Northern Hemisphere during the warmest months of the year, almost exclusively in June–August. The deepest systems occur in June and July, the time of year when the solar heating is maximum. During the warm season, these extreme convective events tend strongly to occur when the surface air temperature and moisture content are at their highest and being advected into high latitudes by southerly wind components, leading to high values of CAPE. They also occur generally during the warmest part of the day, although the diurnal variability is hard to determine from GPM snapshots.

The echo intensities defining these convective events (≥40 dBZ throughout a large volume of echo) are very high, similar in intensity to extreme convective storms seen at lower latitudes (Houze et al., 2015). Most of these convective storms are of the wide type (~78%), indicating that they have achieved mesoscale organization. The maximum heights of the intense echoes may be somewhat restricted by the low tropopause at high latitudes, and possibly other factors such as less extreme surface temperature and humidity that at lower latitudes. Nevertheless, CAPE values can be in the thousands of Joules per kilogram, and 13% of the extreme convective storms are of the DCC type, which have 40-dBZ radar echo cores exceeding 10-km altitude. Above these echo cores, hydrometeors are being carried much higher, potentially impacting stratosphere composition.

In summary, deep, intense, and mesoscale convection has been occurring where Earth's warming has been greatest—namely, over high-latitude continental regions. This type of convection has substantial effects on severe weather, precipitation, and stratospheric interaction in the high-latitude climate. Because the GPM satellite is relatively new, it cannot be determined if the amount of convection at high latitudes has increased, though the statistics are suggestive. The question now arises whether intense convection at high latitudes will become more common as these regions continue to warm.

Acknowledgments
J. Fan, Z. Feng, and J. Wang were supported by Climate Model Development and Validation (CMDV) program of the Department of Energy's Climate and Environmental Sciences Division. R. Houze and S. Brodzik were supported by the Pacific Northwest National Laboratory (PNNL) subcontracts MA243766-TO358850 (CMDV) and MA243766-TO292896 (Water Cycle and Climate Extremes). This research used resources of the National Energy Research Scientific Computing Center (NERSC), a U.S. Department of Energy Office of Science User Facility operated under contract DE-AC02-05CH11231. PNNL is operated for the U.S. Department of Energy (DOE) by Battelle Memorial Institute under contract DE-AC05-76RL01830. The Merged Land-Ocean Surface Temperature Analysis data used in the global temperature analysis are available online (https://www.ncdc.noaa.gov/dataaccess/marineoceandata/noaa-global-surface-temperaturenoaaglobaltemp). The GPM Ku-band radar reflectivity data, as well as the echo object identification results and detailed algorithm, are available at the University of Washington GPM-Ku Dataset website (http://gpm.atmos.washington.edu/). The ERA-Interim data can be obtained at the ECMWF website (https://www.ecmwf.int/en/forecasts/datasets/archive-datasets/reanalysis-datasets/era-interim).

References

Awaka, J., Iguchi, T., Kumagai, H., & Okamoto, K. (1997). Rain type classification algorithm for TRMM precipitation radar. In *Proc. IEEE 1997 Int. Geoscience and Remote Sensing Symp.* (pp. 1633–1635). Singapore, Japan: Institute of Electrical and Electronics Engineers.

Dee, D. P., Uppala, S. M., Simmons, A. J., Berrisford, P., Poli, P., Kobayashi, S., et al. (2011). The ERA-Interim reanalysis: Configuration and performance of the data assimilation system. *Quarterly Journal of the Royal Meteorological Society*, *137*(656), 553–597. https://doi.org/10.1002/qj.828

Feng, Z., Leung, L.-Y., Hagos, S., Houze, R. A. Jr., Burleyson, C., & Balaguru, K. (2016). More frequent intense and long-lived storms dominate the springtime trend in central U.S. rainfall. *Nature Communications*, *7*(1). https://doi.org/10.1038/NCOMMS13429

Gartzke, J., Knuteson, R., Przybyl, G., Ackerman, S., & Revercomb, H. (2017). Comparison of satellite-, model-, and radiosonde-derived convective available potential energy in the southern great plains region. *Journal of Applied Meteorology and Climatology*, *56*(5), 1499–1513. https://doi.org/10.1175/JAMC-D-16-0267.1

Groenemeijer, P., Púčik, T., Holzer, A. M., Antonescu, B., Riemann-Campe, K., Schultz, D. M., et al. (2017). Severe convective storms in Europe: Ten years of research and education at the European Severe Storms Laboratory. *Bulletin of the American Meteorological Society*, *98*(12), 2641–2651. https://doi.org/10.1175/BAMS-D-16-0067.1

Houze, R. A. Jr. (2004). Mesoscale convective systems. *Reviews of Geophysics*, *42*, RG4003. https://doi.org/10.1029/2004RG000150

Houze, R. A. Jr. (2018). 100 years of research on mesoscale convective systems. *Meteorological Monographs*, *59*, 17.1–17.54. https://doi.org/10.1175/AMSMONOGRAPHS-D-18-0001.1

Houze, R. A. Jr., Rasmussen, K. L., Zuluaga, M. D., & Brodzik, S. R. (2015). The variable nature of convection in the tropics and subtropics: A legacy of 16 years of the Tropical Rainfall Measuring Mission satellite. *Reviews of Geophysics*, *53*, 994–1021. https://doi.org/10.1002/2015RG000488

Houze, R. A. Jr., Wilton, D. C., & Smull, B. F. (2007). Monsoon convection in the Himalayan region as seen by the TRMM precipitation radar. *Quarterly Journal of the Royal Meteorological Society*, *133*, 1389–1411. https://doi.org/10.1002/qj.106

Iguchi, T., Seto, S., Meneghini, R., Yoshida, N., Awaka, J., Le, M., et al. (2017). GPM/DPR level-2. Algorithm Theoretical Basis Doc. (68 pp.). Retrieved from https://pmm.nasa.gov/sites/default/files/document_files/ATBD_DPR_201708_whole_1.pdf

Liu, N., & Liu, C. (2016). Global distribution of deep convection reaching tropopause in 1 year GPM observations. *Journal of Geophysical Research: Atmospheres*, *121*, 3824–3842. https://doi.org/10.1002/2015JD024430

Moncrieff, M. W., & Miller, M. J. (1976). The dynamics and simulation of tropical cumulonimbus and squall lines. *Quarterly Journal of the Royal Meteorological Society*, *102*(432), 373–394. https://doi.org/10.1002/qj.49710243208

Sobel, A. H., & Camargo, S. J. (2011). Projected future seasonal changes in tropical summer climate. *Journal of Climate*, *24*, 473–487. https://doi.org/10.1175/2010JCLI3748.1

Vose, R. S., Arndt, D., Banzon, V. F., Easterling, D. R., Gleason, B., Huang, B., et al. (2012). NOAA's merged land-ocean surface temperature analysis. *Bulletin of the American Meteorological Society*, *93*, 1677–1685. https://doi.org/10.1175/BAMS-D-11-00241.1

Wuebbles, D. J., Fahey, D. W., Hibbard, K. A., DeAngelo, B., Doherty, S., Hayhoe, K., et al. (2017). Executive summary. In D. J. Wuebbles, D. W. Fahey, K. A. Hibbard, D. J. Dokken, B. C. Stewart, & T. K. Maycock (Eds.), *Climate science special report: Fourth national climate assessment* (Vol. 1, pp. 12–34). Washington, DC: U.S. Global Change Research Program.

Xie, S., Zhang, Y., Giangrande, S. E., Jensen, M. P., McCoy, R., & Zhang, M. (2014). Interactions between cumulus convection and its environment as revealed by the MC3E sounding array. *Journal of Geophysical Research: Atmospheres*, *119*, 11,784–11,808. https://doi.org/10.1002/2014JD022011